

Journal of Materials Chemistry A

Accepted Manuscript



This is an *Accepted Manuscript*, which has been through the Royal Society of Chemistry peer review process and has been accepted for publication.

Accepted Manuscripts are published online shortly after acceptance, before technical editing, formatting and proof reading. Using this free service, authors can make their results available to the community, in citable form, before we publish the edited article. We will replace this *Accepted Manuscript* with the edited and formatted *Advance Article* as soon as it is available.

You can find more information about *Accepted Manuscripts* in the [Information for Authors](#).

Please note that technical editing may introduce minor changes to the text and/or graphics, which may alter content. The journal's standard [Terms & Conditions](#) and the [Ethical guidelines](#) still apply. In no event shall the Royal Society of Chemistry be held responsible for any errors or omissions in this *Accepted Manuscript* or any consequences arising from the use of any information it contains.

The combination of a new organic D- π -A dye with different organic hole-transport materials for efficient solid-state dye-sensitized solar cells

Peng Liu¹, Bo Xu², Martin Karlsson¹, Jinbao Zhang³, Nick Vlachopoulos³, Gerrit Boschloo³, Licheng Sun², Lars Kloo^{1*}

1. *Applied Physical Chemistry, Center of Molecular Devices, Department of Chemistry, School of Chemical Science and Engineering, KTH-Royal Institute of Technology, SE-10044 Stockholm, Sweden*

2. *Organic Chemistry, Center of Molecular Devices, Department of Chemistry, School of Chemical Science and Engineering, KTH-Royal Institute of Technology, SE-10044 Stockholm, Sweden*

3. *Department of Chemistry-Ångström Laboratory, Physical Chemistry, Uppsala University, SE-75120 Uppsala, Sweden*

Corresponding Author: Lakloo@kth.se

Abstract:

A new organic donor- π -acceptor sensitizer MKA253 has been applied for highly efficient solid-state dye-sensitized solar cells (ssDSSCs). Using 2,2',7,7'-tetrakis (N,N-di-p-methoxyphenyl-amine) 9,9'-spirobifluorene (Spiro-OMeTAD) as the hole transport material (HTM), excellent power conversion efficiency of 6.1% was recorded together with a high short-circuit current of 12.4 mA/cm² under standard AM 1.5G illumination (100 mW cm⁻²). Different combinations of dyes and HTMs have also been investigated in ssDSSC device. The results showed that, small molecule HTM based-devices suffer from comparably high electron recombination losses, thus causing low open-circuit voltage. In addition, photo-induced absorption (PIA) spectroscopy showed that the small-molecule HTMs lead to more efficient dye regeneration in comparison with Spiro-OMeTAD, despite a lower thermodynamic driving force. The results of this study also show that optimized energy levels for the dye/HTMs could be a vital factor for highly efficient ssDSSCs.

1. Introduction

Dye sensitized solar cells (DSSCs) represent promising renewable energy conversion devices because of their potential to low fabrication costs, environmentally friendly features, and excellent conversion efficiency. As originally reported in 1991, by O'Regan and Grätzel¹, incident light is absorbed by a dye that is chemically attached to a mesoporous semiconductor substrate, typically consisting of anatase titanium dioxide. Upon light-induced excitation, the dye molecules inject electrons into the conduction band of the titanium dioxide, leaving the holes in the dye molecules. The electrolyte redox couples or, alternatively, a hole transport material (HTM) subsequently transport the holes to the counter electrodes, thus regenerating the dye molecules. For decades, many scientists and researchers have made significant effort to make highly efficient DSSCs²⁻⁴. The DSSCs based on liquid electrolytes have achieved conversion efficiencies of over 10% based on ruthenium dyes⁵, and metal-free organic dyes^{4, 6, 7}. Recently, the best performing DSSCs exhibit a power conversion efficiency of 13% containing a porphyrin dye and an electrolyte based on a cobalt redox shuttle⁸, providing an efficient mechanism for the hole transport. However, the liquid cells suffer from potential leakage and corrosion problems associated with the volatile and corrosive nature of the liquid electrolyte. In an effort to address these issues, solid-state HTMs have been developed to replace the liquid electrolyte by scientists⁹⁻¹¹. In 2011, ssDSSCs with a record 7.2% efficiency was reported by Grätzel and co-workers, and the cells were based on the HTM 2,2',7,7'-tetrakis(N,N-di-p-methoxyphenylamine) 9,9'-spirobifluorene (spiro-OMeTAD) employing a cobalt complex dopant and custom-synthesized dyes¹². Lately, In Chung et al. have reported the p-type inorganic semiconductor CsSnI_{3-x}F_x as HTM improving the power conversion efficiencies up to 10.2 %¹³. Recently, solid-state perovskite solar cell with more than 15% power conversion efficiency have drawn lots of attentions¹⁴⁻¹⁶.

Currently, insufficient pore filling of the HTM into the relatively thick mesoporous titanium dioxide film has limited the ssDSSCs performance. Due to the short diffusion length and incomplete pore filling, the ssDSSCs are consequently limited to very thin semiconductor substrate films¹⁷⁻¹⁹. Therefore, dyes with wide absorption range and high molar extinction coefficients are necessary in order to achieve a sufficient light harvesting efficiency for high-performing solar cells^{20, 21}. The organic donor- π -acceptor (D- π -A) dyes have drawn significant attention because of their high light harvest ability and low raw material cost²²⁻²⁴. Typically, the donor part is a unit that readily is excited by incoming light, the π part

is the linker consisting of a conjugated system, and finally the acceptor part can act as an electron-withdrawing unit and an anchoring site to the substrate at the same time. It was previously reported that organic dyes based on a triphenylamine (TPA) based donor part are excellent for ssDSCs, due to their good electron-donating ability and fast charge transfer at the dye-HTM interface^{23, 25}. Thus, these organic dyes allow thinner device designs and promising photovoltaic performance.

Hole-transport materials have played a significant role in ssDSSCs. Spiro-OMeTAD, because of its good solubility in common solvents and accessibility (in spite of its high cost), has become a well-known HTM used in ssDSSCs^{12, 26, 27}. However, due to the disadvantage of high cost, low conductivity and relatively poor infiltration into the metal-oxide film, much effort has been made to find alternatives to replace Spiro-OMeTAD²⁸⁻³¹. Recently, Lei, Xu, Sun, Hagfeldt and co-workers used a small-molecule hole-transport material (MeO-TPD) to obtain 4.8% conversion efficiency after a 30 min light-soaking procedure³². Eunkyong Kim and his coworkers introduced in situ solid state polymerization of conducting polymers for highly efficient ssDSSCs³³. Xu, Tian, Hagfeldt and Sun developed a triphenylamine-based oligomer hole-transport material introduced into ssDSSCs and obtained 5.8% conversion efficiency³⁴, and they lately improved the efficiency up to 6.0% by using carbazole-based HTMs under standard AM 1.5 solar light irradiation³⁵. Zhang, Vlachopoulos and co-workers applied a photoelectrochemical polymerization (PEP) method in order to generate conducting polymers as HTMs and obtained high efficiencies of up to 5.6%^{36, 37}. Recently, Grätzel and co-workers reported a new dye with fluorene donor for liquid type DSSCs and obtained high J_{sc} of 16.2 mA cm⁻²³⁸. In this work, we report a new organic dye MKA253 applied to ssDSSCs, together with the effects of a selection of dye-HTM combinations on the power conversion efficiency. The structures of the materials studied in this work are presented in Figure 1.

2. Experimental Section:

2.1 Chemicals Used

All chemicals were purchased from Sigma-Aldrich unless otherwise indicated. The company Dyenamo AB supplied the dye LEG4³⁹. The synthesis of X1 is following the method described in reference³². More synthesis details can be found in ESI.

2.2 Device Fabrication

Fluorine-doped tin dioxide (FTO) substrates were dipped into a Zn-HCl solution (Zinc powder and 2M hydrochloric acid) for etching process in order to form the desired electrode pattern. After that step, the substrates were cleaned in an ultrasonic bath in the following order: deionized water (15 min), acetone (30 min), and ethanol (30 min). A spray pyrolysis deposition (SPD) technique was applied to obtain a compact layer of TiO₂ as a blocking layer on top of the FTO substrate. The solution used in the SPD process was 0.2 M Ti-isopropoxide and 2M acetylacetone in isopropanol, and 10-spray cycle was used as standard procedure. In order to generate the nano-porous TiO₂ film, a TiO₂ paste (Dyesol DSL 18NR-T) mixed with terpineol (2:1 mass ratio) was deposited on the compact layer of TiO₂ using a screen-printing method. After sintering on a hotplate at 500 °C for 30 min and cooling to room temperature, the substrate was immersed into a solution of 0.2 M aqueous TiCl₄ at 70 °C for 30 min. Then, the substrates were rinsed with deionized water and ethanol and annealed on a hotplate at 500 °C for 30 min. After being cooled to 90 °C, the hot TiO₂ film was immersed into a dye bath for 18h. The dye bath solution in this work was 0.2 mM of organic dye (LEG4 or MKA253) in a mixed solvent of tert-butanol and acetonitrile (1:1). After the sensitization, the electrodes were rinsed with ethanol and dried in an N₂ gas flow. The surfaces of the dried substrates were covered by an HTM solution containing additives for 30 s and then spin-coated for 30s at 2000 rpm to form a uniform HTM layer. Afterwards, the cells were left in air overnight in the dark and a 200 nm thick Ag layer was deposited on the top of HTM layer by thermal evaporation in a vacuum chamber (Leica EM MED020).

2.3 Device Characterization

Current-voltage characteristics of the ssDSSCs were studied under 100 mW cm⁻² (AM 1.5) radiation using a Keithley Model 2400 source meter. The light source was calibrated by a certified reference solar cell (Fraunhofer ISE). A black mask with an aperture area of 0.126 cm² was placed on the top of the cell during the measurements. Incident photo-to-current conversion efficiency (IPCE) spectra were recorded by a computer-controlled setup comprised of a xenon lamp (Spectral Products ASB-XE-175), a monochromator (Spectral Products CM110) and a Keithley multimeter (Model 2700), calibrated by a certified reference solar cell (Fraunhofer ISE). The electron lifetime data were recorded through monitoring photovoltaic transients at different light intensities by applying a small square-wave modulation to a base light intensity. The

photovoltaic response was fitted using first-order kinetics in order to obtain the time constants³.

2.4 Photoinduced Absorption Spectroscopy

The solar cell device samples used in photoinduced absorption (PIA) measurements were prepared as described above except the Ag contact layer. PIA spectra were recorded on a in-lab constructed setup⁴⁰. A 20W tungsten-halogen lamp, filtered up to 530 nm, generated the white probe light. A square-wave modulated (on-off) green light source (Lasermate GML532-100FLE, 532nm) was used for excitation. The transmitted probe light was focused onto a monochromator and detected by a UV-enhanced silicon and germanium photodiode detector. 6.1 mWcm⁻² light intensity and 9.3 Hz modulation frequency were used for the blue LED excitation.

2.5 UV-Vis absorption measurement

UV-Vis absorption measurement was performed using a Lambda 750 UV-Vis spectrophotometer. The signal from FTO/TiO₂ substrate was used as calibration. The thickness of the TiO₂ films studied was around 500 nm.

2.6 Conductivity measurement

Glass substrates without conductive layer were carefully cleaned. Remaining organic residues were removed using 10 min by airbrushing. A thin layer of nanoporous TiO₂ was coated onto the glass substrates by spin-coating using a diluted TiO₂ paste (Dyesol DSL 18NR-T) with terpineol (1:3, mass ratio). The thickness of the film is ca. 500 nm, as measured using a DekTak profilometer. The concentrations of the HTM solutions were the same as used for the photovoltaic devices. *J-V* characteristics were recorded on a Keithley 2400 Semiconductor Characterization System. Measurements were carried out following the procedure described in a previously published paper³⁷.

3. Results and Discussion:

3.1 Materials Characterization

Figure 2a shows the light absorbance spectra of the two dyes, LEG4 and MKA253, in ethanol solution and adsorbed onto TiO₂ film. Accordingly,

MKA253 shows a broader light absorption range, up to 600 nm, as compared to LEG4. The absorption maximum of LEG4 and MKA253 is 520 nm and 534 nm in ethanol solution, respectively, and 458 nm and 491 nm on TiO₂ film. A blue-shift is observed when the dyes are adsorbed onto the surface of the mesoporous TiO₂ films. Previous studies have shown that a blue-shift of the absorption is found upon deprotonation of the terminal carboxylic group of the dye molecules^{41, 42}. A much broader absorption range indicates better light harvest abilities of a specific dye, which is beneficial for obtaining highly efficient ssDSSCs. In order to make efficient ssDSSCs, one of the most basic requirements for a sensitizer and an HTM is that the HOMO energy level of the HTM should be above (more negative on the Standard Hydrogen Electrode, SHE, scale) that of the sensitizer. Figure 2b shows the energy level alignment of materials used in this paper. The energies of the Spiro-OMeTAD and X1 HOMOs are taken from the previously published paper⁴³. The values of the band gap for the two dyes are estimated from the UV-Vis absorption curves. More details about the experiment methods can be found in the Electronic Supplementary Information (ESI). The HOMO of MKA253 is slightly more negative (SHE scale) in comparison with the LEG4 dye, resulting in a smaller band gap. All HTMs HOMO more negative energy levels (SHE scale) than the sensitizers, which is essential for the dye regeneration procedure and the ability to work as an HTM. However, the HOMO of MKA253 is much closer to that of X1 and X11, indicating a smaller energy driving force. Furthermore, the Spiro-OMeTAD displays a less negative HOMO level as compared to X1 and X11, indicating a higher driving force for the dye regeneration process.

3.2 Photovoltaic properties of ssDSC

The J-V characteristics of the ssDSSC fabricated using the sensitizers (LEG4 and MKA253) and HTMs (Spiro-OMeTAD, X1, and X11) studied at 1 sun illumination under standard global AM 1.5G conditions are shown in Figure 3, with the corresponding photovoltaic parameters summarized in Table 1. For devices based on LEG4 and Spiro-OMeTAD, a high open-circuit potential V_{oc} of 935 mV and a short-circuit current J_{sc} of 8.8 mA/cm² was recorded, yielding power conversion efficiencies (PCEs) of 5.2%. The performance of devices containing LEG4 in combination with X1 or X11 as hole-transport materials, showed V_{oc} , J_{sc} and FF values of 720 and 655 mV, 8.8 and 8.2 mA cm⁻², and 0.67 and 0.55, yielding PCEs of 4.3% and 3.0%, respectively. The devices containing the MKA253 dye and Spiro-OMeTAD showed an excellent efficiency of 6.1%, which can be attributed to the high current of 12.4

mA/cm². The performance of cells containing X1 as HTM is quite similar to that of cells containing X11. The cells based on X1 showed a J_{sc} of 5.8 mA cm⁻², V_{oc} of 680 mV and PCEs of 2.3 %, while the corresponding devices containing X11 showed a V_{oc} of 580 mV and J_{sc} of 4.7 mA cm⁻², resulting in a lower PCE, 1.7%.

The devices based on Spiro-OMeTAD displayed the highest V_{oc} (935 mV) in combination with the LEG4 dye, and the highest J_{sc} (12.4 mA) in combination with the MKA253 dye. For the same sensitizer, the V_{oc} of the solar cell devices decreased in the order Spiro-OMeTAD > X1 > X11. Furthermore, the J_{sc} remained very similar for the devices based on LEG4 in combination with the different HTMs. In contrast, for MKA253, the device J_{sc} dropped dramatically following the order Spiro-OMeTAD > X1 > X11. Therefore, the performance for devices based on MAK253 in combination with X1 and X11 was considerably much poorer than that of o the Spiro-OMeTAD based devices.

3.3 Incident Photon-to-Current Conversion Efficiency

The higher J_{sc} values recorded for devices containing MKA253 in combination with Spiro-OMeTAD arise from the better light-harvesting ability of the dyes, which is evident in the incident-photon-to-current conversion efficiency (IPCE) spectra. The IPCE data are in good agreement with the results shown in Table 1. For ssDSSCs containing Spiro-OMeTAD as HTM, the combination with MKA253 shows a much broader absorption range and the highest maximum monochromatic efficiency (76% at 460 nm), as compared to that of devices containing LEG4. According to the Figure 2a, the MKA253 and LEG4 dyes adsorbed onto a TiO₂ film display an absorption edge at 730 nm and 680 nm, respectively. The better light-harvesting abilities of MK253 thus logically should lead to higher J_{sc} , potentially giving rise to a higher PCE. For devices based on the LEG4 dye, the IPCE curves for the different HTMs are similar, and thus the corresponding J_{sc} are quite similar. However, for devices based on the MKA253 dye, the IPCE spectra for devices based on X1 and X11 as HTMs are much lower than those based on the LEG4 dye, consequently resulting lower J_{sc} , in spite of the potentially superior light-harvest abilities of MKA253.

There are many factors that can affect the resulting device current. One of those could be that the relative energy alignment of the dyes and the hole-transport materials do not favor the energy or the electron transfers, resulting in a less efficient dye regeneration process. In general, the driving force for dye regeneration mainly arises from the energy difference between the HOMO energy level of the dye and the HTM. From Figure 1b , we can note that the HOMO energy level of X1 and

X11 is much closer to that of MKA253, if compared with that of Spiro-OMeTAD. Therefore, the dye regeneration for MKA253 may not be sufficiently efficient in devices combining the dye with X1 and X11 as the HTM. This aspect will be discussed further below.

3.4 Electron Lifetime Measurement

Recombination losses of the injected photoelectrons is one of the key factors that affects the performance of ssDSSCs. A longer electron lifetime indicates a lower recombination loss rate of the photogenerated charges, typically observed in terms of a higher V_{oc} . In Figure 5, the electron lifetimes of different dye-sensitized devices are plotted versus V_{oc} . The devices based on the LEG4 dye in combination with Spiro-OMeTAD showed the longest electron lifetime, while those based on MKA253 in combination with X11 presented the shortest electron lifetime. In general, the V_{oc} of ssDSSCs is determined by the difference between the oxidation potential of the HTM and the quasi-Fermi level of TiO_2 . A shorter electron lifetime is expected to give a lower V_{oc} , since a higher degree of recombination losses would render a lower quasi-Fermi level⁴⁴. With this in mind, the shorter electron lifetimes observed are in good agreement with the V_{oc} data shown in Table 1. For devices containing Spiro-OMeTAD as the HTM, the lifetime in combination with LEG4 is much longer than for those in combination with MKA253. The reason can be speculated to be associated with the less rigid donor part of LEG4 and possible effects on the recombination loss rate.

For the same sensitizer, similar trends can be noted: the electron lifetime for devices based on Spiro-OMeTAD is typically significantly longer than those based on X11 or X1. In spite of the fact that the more positive (SHE scale) HOMO energy level of X11 and X1 could result in a higher V_{oc} (Figure 2b), a better pore-filling ability of the small-molecular HTMs may instead enhance the recombination loss process between injected electrons and the oxidized HTM. The present results indicate that there is a delicate balance between beneficial and detrimental effects expected from HTMs based on small molecules.

3.5 Photo-induced Absorption Spectroscopy

In order to study the regeneration process of the oxidized dye molecules by the hole transport materials, photo-induced absorption (PIA) spectroscopy was performed. Figure 8a shows the absorption range between 700 and 800 nm, which arise from the oxidized state of LEG4. After deposition of the HTM onto a TiO_2 /LEG4 film, the decrease intensity of absorption in this range is attributed to the dye regeneration

process. Thus, it is clear that the absorption intensity at 700-800 nm decreased due to the dye regeneration in all cases. In general, the PIA curves of devices containing different HTMs did not show significant differences. However, between 700 and 750 nm, the PIA spectra of the combinations $\text{TiO}_2/\text{LEG4}/\text{X11}$ and $\text{TiO}_2/\text{LEG4}/\text{X1}$ are more reduced as compared with that of $\text{TiO}_2/\text{LEG4}/\text{Spiro-OMeTAD}$, indicating faster dye regeneration of the former HTMs. From Figure 2b, we can see the driving force of dye regeneration for Spiro-OMeTAD is expected to be stronger than for the other two HTMs. This result may indicate yet another delicate balance in the devices; HTMs based on smaller molecules may be more easily infiltrated into the mesoporous TiO_2 pores, leading to more efficient dye regeneration in spite of a lower thermodynamic driving force.

Figure 8b shows the PIA spectra of MKA253-sensitized TiO_2 films with and without HTM added. Here, we can note that the absorption between 650 and 850 nm arise from the oxidized state of the MKA253 dye molecules. For all three HTMs in combination with MKA253, the absorption intensity at 650-850 nm decreases, indicating an efficient dye regeneration process. Moreover, between 700 and 800 nm, a slightly smaller effect was observed for the combinations with X1 and X11, as compared to that of Spiro-OMeTAD. Therefore, the MKA253/Spiro-OMeTAD appears to show the fastest dye regeneration process. The reason could be attributed to the extremely low driving force of dye regeneration in the MKA253/X1 and MKA253/X11 systems. As seen in Figure 2b, the very similar HOMO energy levels of X1 and X11 with respect to that of MKA253 may restrict the driving force for the dye regeneration. Therefore, the energy driving force is a vital factor to consider when searching for new HTMs to solar cells containing the MKA253 dye.

3.6 Theoretical Calculations

In order to gain insight into the electronic and optical properties of the investigated dyes, DFT/TDDFT calculations were performed. Details of the calculation are given in the ESI. The geometrically optimized dye molecules and their frontier orbitals are shown in Figure 7. The dyes LEG4 and MKA253 display the typical HOMO-LUMO pattern of the family of D- π -A dyes, where the LUMO is mainly localized on the acceptor moiety and the HOMO is mainly localized on the donor and bridge part of the molecules. From the TDDFT calculations, the lowest transition energies for protonated (deprotonated) LEG4 and MKA253 in formal gas phase are 493 (437) nm and 588 (496) nm, respectively, which are in good agreement with the experimentally observed UV-Vis

absorption maxima. Furthermore, calculational results reproduced the absorption maximum trend, showing a slight red-shift going from LEG4 to MKA253.

The hole-transport rate between the dye molecules and the hole-transport materials can be one of the most important factors affecting the performance of the ssDSSCs. Non-adiabatic Marcus theory is used to estimate the charge-transfer rate⁴⁵, M :

$$M = \frac{2\pi}{\hbar} \frac{|g|^2}{\sqrt{4\pi\lambda k_B T}} e^{-\frac{(\Delta G_0 + \lambda)^2}{4k_B T}},$$

where g describes the electronic coupling, ΔG_0 is the difference in free energy between the equilibrium states of the products and reactants, and λ is the re-organization energy. According to the Marcus theory, the re-organization energy is an important factor determining the hole-transport rate. Here, we calculated the re-organization energy of the dye and the HTM used in this work (Table 2). It is notable that the re-organization energy of MKA253 dye is smaller than that of LEG4. Therefore, the hole after excitation and electron injection into the TiO_2 substrate can be more readily transported through MKA253 dye multiple layers, indicating the regeneration process by the HTM to be facilitated. The lower re-organization energy observed could explain the high J_{sc} 's observed for the MKA253/Spiro-OMeTAD-based solar cells.

For solid-state dye-sensitized solar cells, the hole-hopping process between the molecules constituting the materials also must affect the overall performance. From the calculation, the re-organization energy of Spiro-OMeTAD can be noted to be much lower than for the other two materials, indicating better transport abilities (Table 2). The results from conductivity measurements also support this hypothesis. From the data in Table 3, the hole conductivity of Spiro-OMeTAD, X1 and X11 films are $1.37 \times 10^{-4} \text{ S cm}^{-1}$, $5.3 \times 10^{-5} \text{ S cm}^{-1}$, and $4.2 \times 10^{-5} \text{ S cm}^{-1}$, respectively. The high conductivity of Spiro-OMeTAD is expected to reduce the charge transport resistance in the ssDSSC devices and in this way improve the FF.

4. Conclusion:

A new organic donor- π -acceptor dye, MKA253, has been investigated in ssDSSCs. Devices based on the new MKA253 dye in combination with Spiro-OMeTAD as hole-transport material yield impressive short-circuit currents of up to 12.4 mA/cm^2 , and a resulting power conversion

efficiency of 6.1%. In comparison with the LEG4 dye, the MKA253 dye shows a broader absorption range and higher IPCE values from the resulting ssDSSC devices. Computational studies show that the re-organization energy of the MKA253 dye is much lower than that of the LEG4 dye. The lower re-organization energy may favor the hole-hopping process between multi-layers of dyes and also between the dyes and an HTM, resulting more efficient dye regeneration.

The compatibility of the specific combinations of HTMs and sensitizers is an essential factor to consider when designing new ssDSSCs. Hole-conductor materials based on small molecules have been also investigated in this paper. For the same HTM, the devices based on fluorene donor dyes show much shorter electron lifetimes, compared with ones based on LEG4 dye. For LEG4 dye, the small molecular size of the hole transport material shows similar efficiency of dye regeneration, in comparison with Spiro-OMeTAD. However, the smaller enhance the recombination between the TiO₂ film and HTM, resulting shorter electron life-time. For the MKA253 dye, the combination with X1 and X11 indicate an inefficient dye regeneration process as a result of a low thermodynamic driving force. Therefore, energy level alignment is an essential factor to consider when designing highly efficient solid-state dye-sensitized solar cells.

Acknowledgements:

The Swedish Research Council, the Swedish Energy Agency, the Chinese Scholarship Council (CSC) and Knut and Alice Wallenberg Foundation are gratefully acknowledged for their financial support.

References:

1. B. O'Regan and M. Gratzel, *Nature*, 1991, 353, 737-740.
2. A. Hagfeldt and M. Grätzel, *Accounts of Chemical Research*, 2000, 33, 269-277.
3. A. Hagfeldt, G. Boschloo, L. Sun, L. Kloo and H. Pettersson, *Chemical Reviews*, 2010, 110, 6595-6663.
4. A. Yella, H.-W. Lee, H. N. Tsao, C. Yi, A. K. Chandiran, M. K. Nazeeruddin, E. W.-G. Diao, C.-Y. Yeh, S. M. Zakeeruddin and M. Grätzel, *Science*, 2011, 334, 629-634.
5. Q. Yu, Y. Wang, Z. Yi, N. Zu, J. Zhang, M. Zhang and P. Wang, *ACS nano*, 2010, 4, 6032-6038.

6. L. Alibabaei, J. H. Kim, M. Wang, N. Pootrakulchote, J. Teuscher, D. Di Censo, R. Humphry-Baker, J. E. Moser, Y. J. Yu, K. Y. Kay, S. M. Zakeeruddin and M. Grätzel, *Energy & Environmental Science*, 2010, 3, 1757-1764.
7. S. Haid, M. Marszalek, A. Mishra, M. Wielopolski, J. Teuscher, J.-E. Moser, R. Humphry-Baker, S. M. Zakeeruddin, M. Grätzel and P. Bäuerle, *Advanced Functional Materials*, 2012, 22, 1291-1302.
8. S. Mathew, A. Yella, P. Gao, R. Humphry-Baker, F. E. Curchod, N. Ashari-Astani, I. Tavernelli, U. Rothlisberger, K. Nazeeruddin and M. Grätzel, *Nat Chem*, 2014, 6, 242-247.
9. L. Bin, W. Liduo, K. Bonan, W. Peng and Q. Yong, *Solar Energy Materials and Solar Cells*, 2006, 90, 549-573.
10. U. Bach, D. Lupo, P. Comte, J. E. Moser, F. Weissortel, J. Salbeck, H. Spreitzer and M. Grätzel, *Nature*, 1998, 395, 583-585.
11. N. Cai, S.-J. Moon, L. Cevey-Ha, T. Moehl, R. Humphry-Baker, P. Wang, S. M. Zakeeruddin and M. Grätzel, *Nano Letters*, 2011, 11, 1452-1456.
12. J. Burschka, A. Dualeh, F. Kessler, E. Baranoff, N.-L. L. Cevey-Ha, C. Yi, M. K. Nazeeruddin and M. Grätzel, *Journal of the American Chemical Society*, 2011, 133, 18042-18045.
13. I. Chung, B. Lee, J. He, R. P. Chang and M. G. Kanatzidis, *Nature*, 2012, 485, 486-489.
14. J. Burschka, N. Pellet, S.-J. J. Moon, R. Humphry-Baker, P. Gao, M. K. Nazeeruddin and M. Grätzel, *Nature*, 2013, 499, 316-319.
15. H.-S. S. Kim, C.-R. R. Lee, J.-H. H. Im, K.-B. B. Lee, T. Moehl, A. Marchioro, S.-J. J. Moon, R. Humphry-Baker, J.-H. H. Yum, J. E. Moser, M. Grätzel and N.-G. G. Park, *Scientific reports*, 2012, 2, 591.
16. N. J. Jeon, J. H. Noh, Y. C. Kim, W. S. Yang, S. Ryu and S. I. Seok, *Nature Materials*, 2014, DOI: 10.1038/nmat4014, 897-903.
17. M. Wang, J. Liu, N.-L. Cevey-Ha, S.-J. Moon, P. Liska, R. Humphry-Baker, J.-E. Moser, C. Grätzel, P. Wang, S. M. Zakeeruddin and M. Grätzel, *Nano Today*, 2010, 5, 169-174.
18. J. S. Henry, H.-B. Robin, C. Peter, C. Ilkay, M. Z. Shaik and G. Michael, *Nanotechnology*, 2008, 424003.
19. F. Fabregat-Santiago, J. Bisquert, L. Cevey, P. Chen, M. Wang, S. M. Zakeeruddin and M. Grätzel, *Journal of the American Chemical Society*, 2009, 131, 558-562.
20. J. S. Henry, P. Annamaria, I. Seigo, M. Hidetoshi and G. Michael, *Advanced Functional Materials*, 2009, DOI: 10.1002/adfm.200801751, 1810-1818.
21. P. Chen, J. H. Yum, F. De Angelis, E. Mosconi, S. Fantacci, S.-J. J. Moon, R. H. Baker, J. Ko, M. K. Nazeeruddin and M. Grätzel, *Nano letters*, 2009, 9, 2487-2492.
22. L. Kloo, *Chemical Communications*, 2013, 49, 6580-6583.
23. X. Jiang, K. Karl Martin, E. Gabrielsson, E. M. J. Johansson, M. Quintana, M. Karlsson, S. Licheng, G. Boschloo and H. Anders, *Advanced Functional Materials*, 2011, 21, 2944-2952.
24. D. P. Hagberg, T. Edvinsson, T. Marinado, G. Boschloo, A. Hagfeldt and L. Sun, *Chemical Communications*, 2006, DOI: 10.1039/B603002E, 2245-2247.

25. Y. Jun-Ho, P. H. Daniel, M. Soo-Jin, K. Karl Martin, M. Tannia, S. Licheng, H. Anders, K. N. Mohammad and G. Michael, *Angewandte Chemie International Edition*, 2008, DOI: 10.1002/anie.200804719, 1576-1580.
26. H. J. Snaith, A. J. Moule, C. Klein, K. Meerholz, R. H. Friend and M. Grätzel, *Nano letters*, 2007, 7, 3372-3376.
27. W. Mingkui, X. Mingfei, S. Dong, L. Renzhi, G. Feifei, Z. Guangliang, Y. Zhihui, H.-B. Robin, W. Peng, M. Z. Shaik and G. Michael, *Advanced Materials*, 2008, DOI: 10.1002/adma.200801178, 4460-4463.
28. T. Leijtens, I. K. K. Ding, T. Giovenzana, J. T. Bloking, M. D. McGehee and A. Sellinger, *ACS nano*, 2012, 6, 1455-1462.
29. H. Wang, X. Zhang, F. Gong, G. Zhou and Z.-S. Wang, *Advanced Materials*, 2012, 24, 121-124.
30. J. E. Kroeze, N. Hirata, L. Schmidt-Mende, C. Orizu, S. D. Ogier, K. Carr, M. Grätzel and J. R. Durrant, *Advanced Functional Materials*, 2006, 16, 1832-1838.
31. B.-w. Park, L. Yang, E. M. J. Johansson, N. Vlachopoulos, A. Chams, C. Perruchot, M. Jouini, G. Boschloo and A. Hagfeldt, *The Journal of Physical Chemistry C*, 2013, 117, 22484-22491.
32. L. Yang, B. Xu, D. Bi, H. Tian, G. Boschloo, L. Sun, A. Hagfeldt and E. M. Johansson, *Journal of the American Chemical Society*, 2013, 135, 7378-7385.
33. J. K. Koh, J. Kim, B. Kim, J. H. Kim and E. Kim, *Advanced Materials*, 2011, 23, 1641-1646.
34. B. Xu, H. Tian, D. Bi, E. Gabrielsson, E. M. J. Johansson, G. Boschloo, A. Hagfeldt and L. Sun, *Journal of Materials Chemistry A*, 2013, 1, 14467-14470.
35. B. Xu, E. Sheibani, P. Liu, J. Zhang, H. Tian, N. Vlachopoulos, G. Boschloo, L. Kloo, A. Hagfeldt and L. Sun, *Advanced Materials*, 2014, DOI: 10.1002/adma.201402415, n/a-n/a.
36. J. Zhang, L. Häggman, M. Jouini, A. Jarboui, G. Boschloo, N. Vlachopoulos and A. Hagfeldt, *Chemphyschem : a European journal of chemical physics and physical chemistry*, 2014, DOI: 10.1002/cphc.201301075.
37. J. Zhang, L. Yang, Y. Shen, B.-W. Park, Y. Hao, E. M. J. Johansson, G. Boschloo, L. Kloo, E. Gabrielsson, S. Licheng, A. Jarboui, C. Perruchot, M. Jouini, N. Vlachopoulos and H. Anders, *The Journal of Physical Chemistry C*, 2014, DOI: 10.1021/jp412504s, 580190662.
38. Y. Aswani, H.-B. Robin, F. E. C. Basile, A. Negar Ashari, T. Joël, E. P. Lauren, M. Simon, E. M. Jacques, T. Ivano, R. Ursula, G. Michael, N. Md. Khaja and F. Julien, *Chemistry of Materials*, 2013, 25, 2733-2739.
39. E. Gabrielsson, H. Ellis, S. Feldt, H. Tian, G. Boschloo, H. Anders and S. Licheng, *Advanced Energy Materials*, 2013, 3, 16471656.
40. G. Boschloo and A. Hagfeldt, *Inorganica Chimica Acta*, 2008, 361, 729-734.
41. M. Pastore, E. Mosconi, F. Angelis and M. tzel, *The Journal of Physical Chemistry C*, 2010, 114, 7205-7212.
42. A. Dualeh, F. D. Angelis, S. Fantacci, T. Moehl, C. Yi, F. Kessler, E. Baranoff, K. N. Mohammad and G. Michael, *The Journal of Physical Chemistry C*, 2012, 116, 15721578.

43. B. Xu, H. Tian, L. Lin, D. Qian, H. Chen, J. Zhang, N. Vlachopoulos, G. Boschloo, Y. Luo, F. Zhang, A. Hagfeldt and L. Sun, *Advanced Energy Materials*, 2014, DOI: 10.1002/aenm.201401185, n/a-n/a.
44. P. Chen, J. H. Yum, F. D. Angelis, E. Mosconi, S. Fantacci, S.-J. Moon, R. H. Baker, J. Ko, M. K. Nazeeruddin and M. Grätzel, *Nano Letters*, 2009, 9, 2487-2492.
45. R. A. Marcus and N. Sutin, *Biochimica Et Biophysica Acta*, 1985, 811, 265-322.

Table 1. Photovoltaic parameters of devices based on different sensitizers and hole-transport materials studied at a light intensity of 100mW cm^{-2} (AM 1.5G).

	Jsc [mA/cm ²]	Voc [mV]	FF	PEC
LEG4/Spiro-OMeTAD	8.8	935	0.63	5.2%
LEG4/X1	8.8	720	0.67	4.3%
LEG/X11	8.2	655	0.55	3.0%
MKA253/Spiro-OMeTAD	12.4	780	0.63	6.1%
MKA253/X1	5.8	680	0.58	2.3%
MKA253/X11	4.7	580	0.62	1.7%

Table 2. Re-organization energies calculated for sensitizers and hole-transport materials.

	MKA253	LEG4	Spiro-OMeTAD	X1	X11
Re-organizaition Energy (meV)	182	206	106	208	221

Table 3. Conductivity of the hole-transport materials.

	Spiro-OMeTAD (30mM)	X1 (60mM)	X11 (60mM)
Conductivity (S cm ⁻¹)	$1.37 \cdot 10^{-4}$	$0.53 \cdot 10^{-4}$	$0.42 \cdot 10^{-4}$

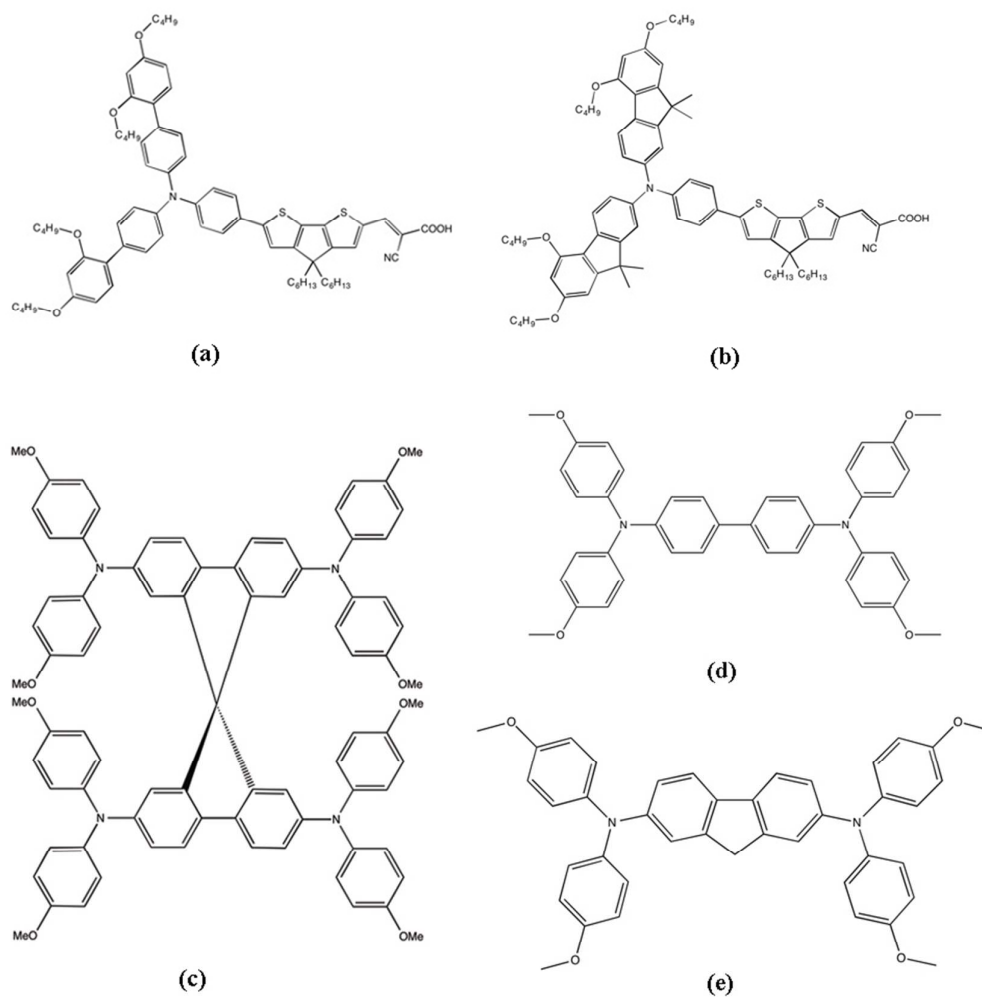


Figure 1. Molecular structures of the different sensitizers (a) LEG4, (b) MKA253, and hole-transport materials: (c) Spiro-OMeTAD, (d) X1, and (e) X11.

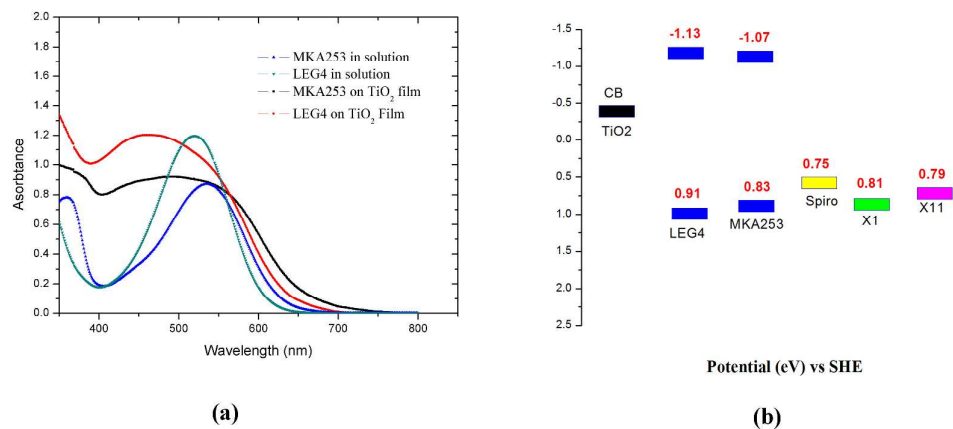


Figure 2. (a) UV-Vis absorption spectra of LEG4 and MKA253 in ethanol solution and on a TiO₂ film. (b) Energy alignment of the HOMO (and for the dyes LUMO) energy levels of the dyes and HTMs on the TiO₂ film studied in this work.

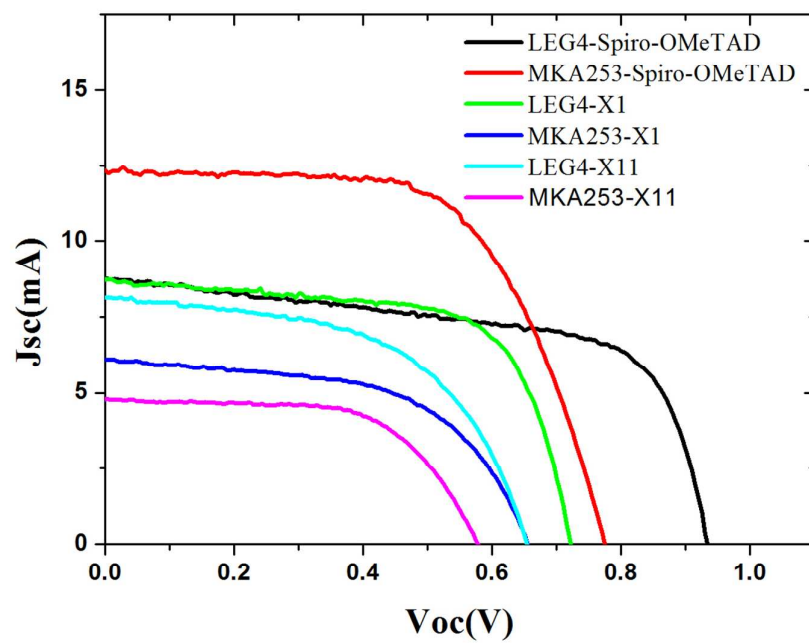


Figure 3. J-V curves of the solid-state dye-sensitized solar cells based on different dyes and hole-transport materials.

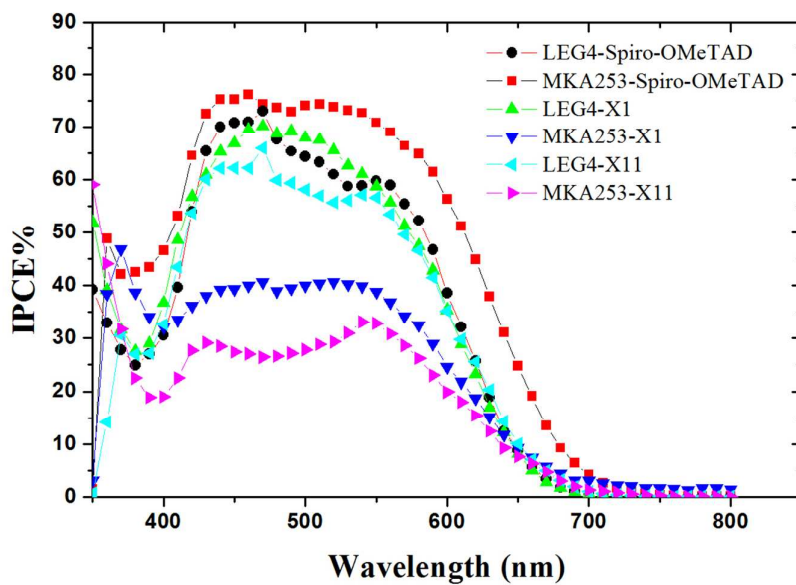


Figure 4. IPCE spectras of the solid-state dye-sensitized solar cells based on different dyes and hole-transport materials.

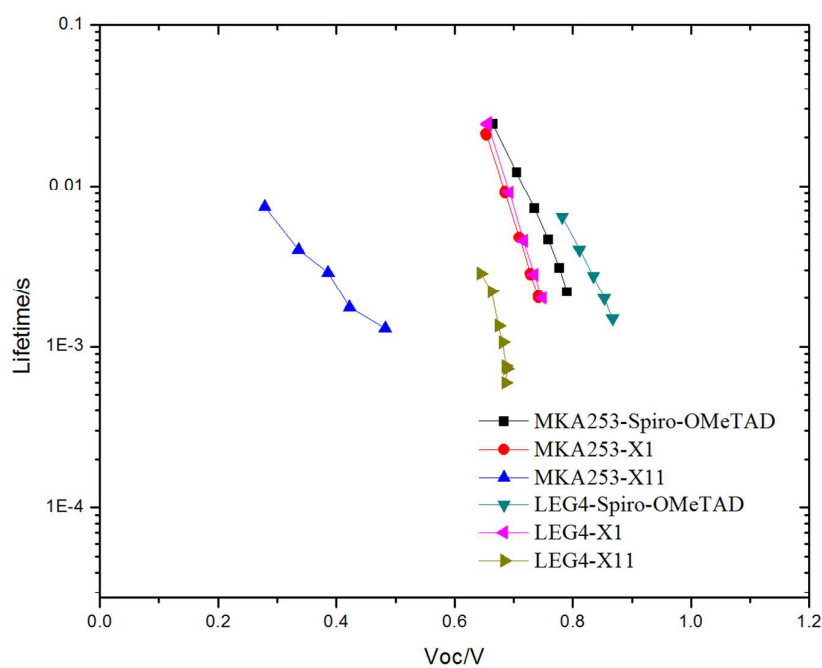


Figure 5. Electron lifetime of different solid-state dye-sensitized solar cells versus the open-circuit potential.

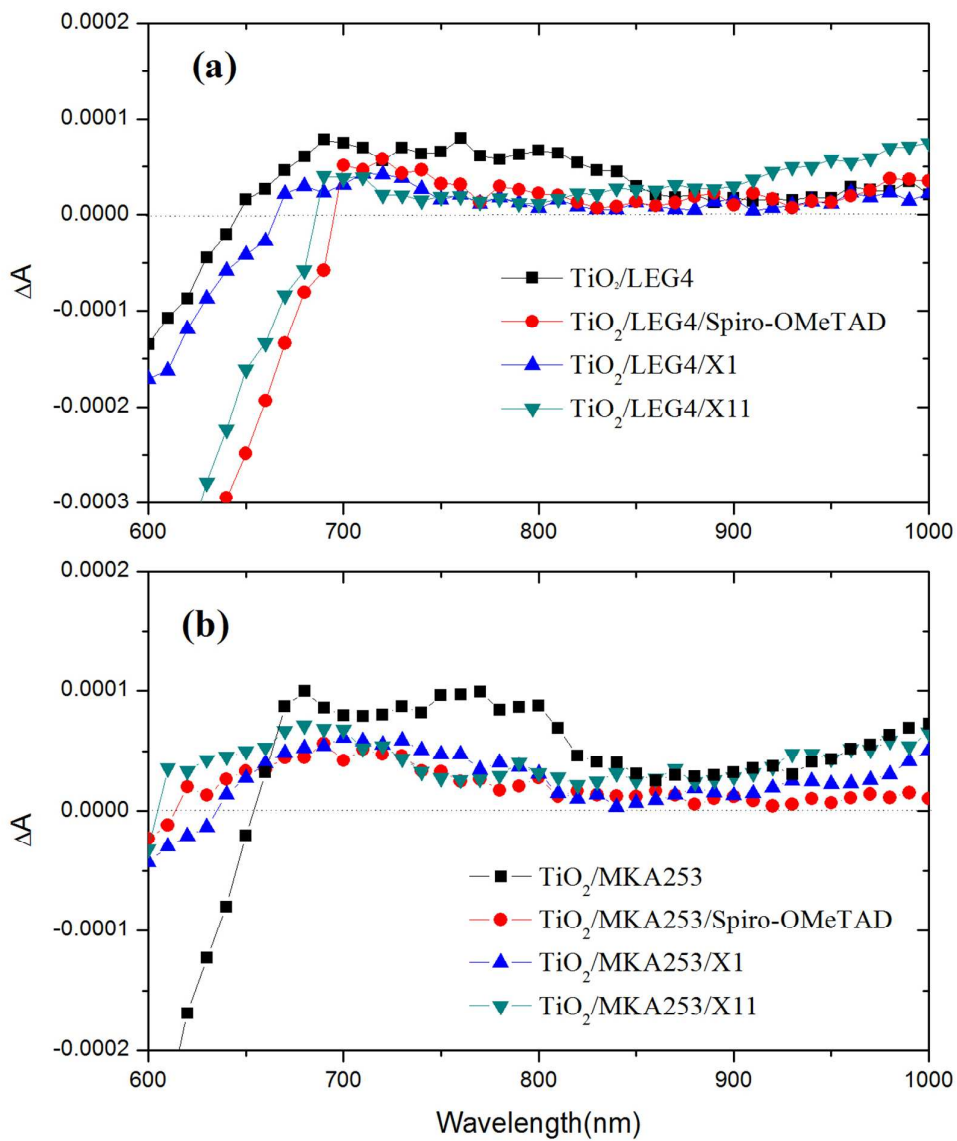


Figure 6. PIA signals of different films based on LEG4 (a), and MKA253 (b).

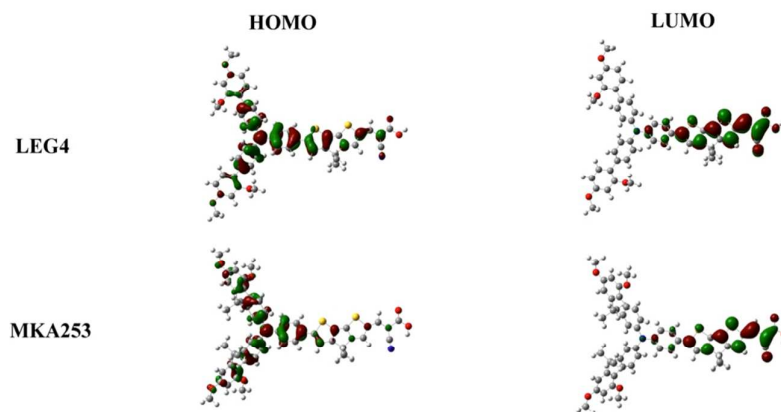


Figure 7. Frontier orbitals of the dyes plotted at an isosurface value of 0.02.

TOC:

